Inorganic Chemistry

pubs.acs.org/IC Article

Can a Nonorganometallic Ruthenium(II) Polypyridylamine Complex Catalyze Hydride Transfer? Mechanistic Insight from Solution Kinetics on the Reduction of Coenzyme NAD^+ by Formate

Marta Chrzanowska, Anna Katafias, and Rudi van Eldik*

Cite This: *Inorg. Chem.* 2020, 59, 14944−14953 Read Online

ACCESS | Metrics & More | Article Recommendations | Supporting Information

ABSTRACT: Application of organometallic ruthenium(II) arene complexes has been successful for the modulation of cellular redox processes via their interaction with species such as formate to control the NAD^+/NADH balance in cells. Here we present the first evidence that similar effects can be reached with the application of a nonorganometallic ruthenium(II) polypyridyl complex. Kinetic studies performed demonstrate the ability of $[Ru^{II}(terpy)(en)(H_2O/EtOH)]^{2+}$ in water/ethanol (1:9, v/v) solution, where terpy = 2,2′:6′,2″-terpyridine and en = ethylenediamine, to catalyze the reduction of the NAD^+ coenzyme to NADH in the presence of formate as hydride transfer source. In this case, terpy instead of arene is responsible for the labilization of coordinated solvent. The suggested catalytic cycle begins with the fast anation of the $[Ru^{II}(terpy)(en)(H_2O/EtOH)]^{2+}$ complex by formate. This is followed by the rate-determining formate-catalyzed decarboxylation of the generated ruthenium(II) formato complex to form $[Ru^{II}(terpy)(en)H]^+$. Rapid hydride transfer to NAD^+ from $[Ru^{II}(terpy)(en)H]^+$ to form NADH and to regenerate the starting ruthenium(II) solvato complex, closes the overall catalytic cycle.

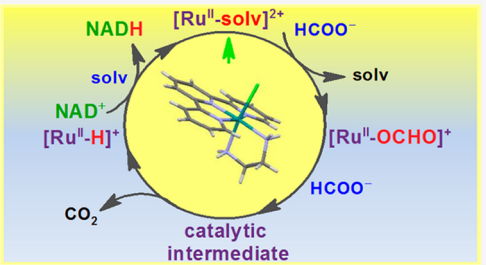

INTRODUCTION

According to the latest reports, many serious diseases plaguing contemporary society are caused by redox imbalance in cells.[1−9] Elucidation of the relationship between oxidative/reductive stress and cellular inflammation, and the development of a so-called redox therapy, is one of the main tasks of the upcoming new discipline of redox biology.[10−17] It deals with the redox imbalance in cells, involves electron transfer of free radicals and nitrogen and oxygen metabolites ($O_2^{\bullet-}$, H_2O_2, $OH^{\bullet}$, $^1O_2$, $NO^{\bullet}$, $ONOO^-$, NO_2, and N_2O_3), and focuses on an important sector of fundamental processes in biology. Reductive stress is defined as a relative shortage of reactive oxygen species (ROS) compared to the reducing equivalents in the form of redox couples such as NAD^+/NADH (where NAD^+ and NADH are nicotinamide adenine dinucleotide and its reduced form, respectively). Accordingly, oxidative stress is caused by an excess of ROS and reactive nitrogen species relative to the reducing equivalents.[18] The effect of chemical modifications on the driving force of redox processes in cells plays a fundamental role in the control of many biological processes such as gene expression, cell cycle progress, and apoptosis, which cause diseases such as cancers, hypertension, atherosclerosis, renal diseases, diabetic neuropathies, and Alzheimer's disease.[19]

Transition-metal complexes can play an important role in the redox biology of cells, as shown recently in a series of papers by Sadler et al.[20−24] Inert organometallic complexes, such as $[Ir^{III}(Cp^*)(N\text{-}C)py]^+$ (Cp^* = pentamethylcyclopentadienyl, N-C = N,C-donor chelating ligand, and py = pyridine) and related complexes of Ru(II/III), Rh(III), Os(II), and Fe(II), can react with NADH as a source of hydride (H^-) to form ROS, such as hydroperoxide, $O_2 + H^- \rightarrow HOO^-$, and cause oxidative stress. In these organometallic complexes, metal−carbon bonds labilize the metal center and induce a high reactivity for the interaction with crucial species such as NADH to control the redox balance and inflammation in living cells. Oxidative stress is an effective method to kill cancer cells because an increase in the level of ROS disturbs redox homeostasis inside cells and causes destruction.[25−30] Furthermore, organometallic complexes of Ru(II) of the pseudooctahedral type can in the presence of formate (as the hydride source) control the $[NAD^+]/[NADH]$ balance and cause reductive stress. Accordingly, these complexes can catalytically reduce NAD^+ in cancer cells and lead to reductive stress, in contrast to organometallic iridium complexes, which induce oxidative stress. In conclusion, organometallic complexes are apparently unique in their ability to achieve redox modulation (oxidative versus reductive stress) in living cells.

Can the application of nonorganometallic complexes of labile metal centers such as ruthenium(II) polypyridylamine com-

Received: June 2, 2020
Published: October 1, 2020

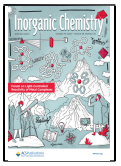

https://dx.doi.org/10.1021/acs.inorgchem.0c01613
Inorg. Chem. 2020, 59, 14944−14953

plexes control the redox balance in living cells? The advantage of nonorganometallic coordination compounds is their biocompatible nature, which is known for many related systems presently used in anticancer treatment, which, in general, is not always the case for organometallic complexes.

In this work, we investigated the ability of a nonorganometallic ruthenium(II) polypyridylamine complex, [Ru(terpy)(en)Cl]Cl (where terpy and en are 2,2′:6′,2″-terpyridine and ethylenediamine, respectively), to catalyze the conversion of NAD^+ to 1,4-NADH using sodium formate as a source of hydride. In this complex, the terpy chelate labilizes the coordinated chloride via π-acceptor properties in a manner similar to the way Cp* and related chelates do in the organometallic complexes mentioned above. Although a large group of polypyridyl complexes of Ru(II) have been known for many years, they have only recently received special attention, among others, for their covalent and supramolecular interactions with DNA and promising cytotoxicity in cell tests, which makes them potential candidates for therapeutics and theranostics.[31−37]

EXPERIMENTAL SECTION

Chemicals. All chemicals were of analytical-reagent grade and were used without further purification. $RuCl_3{\cdot}xH_2O$ was purchased from Acros Organics. Ethylenediamine, 2,2′:6′,2″-terpyridine, lithium chloride, methanol-d_4, sodium formate-d, β-nicotinamide adenine dinucleotide sodium salt, and tris(hydroxymethyl)aminomethane (TRIS) and 2-ethanesulfonic acid (MES) buffers were obtained from Sigma-Aldrich. Sodium formate, tetrahydridoborate, and solvents were purchased from Avantor Performance Materials Poland SA.

Synthesis of the Complex. [Ru(terpy)(en)Cl]Cl was synthesized according to a procedure described earlier.[38] The complex was fully characterized in the solid state and in solution as reported before. Solutions of $[Ru(terpy)(en)(H_2O)]^{2+}$ were prepared by spontaneous aquation of the chlorido parent complex (ca. 7 min) at room temperature.

Instrumentation. UV−vis spectral analyses and kinetic studies were carried out using a conventional Shimadzu UV-1601 PC spectrophotometer combined with a Julabo F25 cryostat (±0.1 °C). Single-wavelength kinetic data were processed with the *EnzFiter* software. To study fast reactions, an Applied Physics SX20 stopped-flow spectrometer with a rapid-scan photodiode-array mode with 1 nm spectral resolution, equipped with a J&M detector and Colora thermostat, was used. ^{1}H NMR spectra were recorded on a Bruker Avance-700 NMR spectrometer in a D_2O/CD_3OD (1:9, v/v) solution; chemical shifts were referenced to tetramethylsilane.

Kinetic Measurements. Reactions of the ruthenium(II) aqua complex with $NaBH_4$ in a water (H_2O)/ethanol (EtOH; 1:9, v/v) solution were initiated by the addition of a small aliquot of aqueous solution of $NaBH_4$ dissolved just before the measurements. Reactions of the ruthenium(II) aqua complex with formate, acetate, and chloride in a H_2O/EtOH (1:9, v/v) solution were initiated by the addition of small aliquots of an aqueous solution of the complex and monitored as an increase in absorbance at 397, 400, and 475 nm, respectively. Both reaction types were followed using conventional methods. The reduction of NAD^+ by $NaBH_4$ was followed using the stopped-flow method at 15.2 ± 0.1 °C in a H_2O/EtOH (1:9, v/v) solution. The formation of NADH was monitored by the characteristic increase in absorbance at 340 nm.

The overall spectral changes accompanying the examined catalytic reactions were recorded within the 300−800 nm wavelength range using a conventional UV−vis spectrophotometer at 36.8 ± 0.1 °C (controlled before and after each experiment) in the presence of air, argon, or CO_2. Reactions were initiated by the addition of small aliquots of a thermostated sodium formate aqueous solution to a thermostated mixture of NAD^+ and the Ru(II) complex in a H_2O/EtOH solution. Measurements were, in general, carried out in a 1:9 (v/v) H_2O/EtOH solution. Additional measurements were performed in 3:7 and 5:5 (v/v) H_2O/EtOH solutions. All experiments were repeated at least two times. Kinetic test experiments were performed in 0.05 M TRIS and MES buffer solutions of pH 7.4 and 7.1, respectively.

NMR Studies. $[Ru(terpy)(en)(H)]^+$ was prepared by the addition of a large excess of $NaBH_4$ to a hot D_2O/CD_3OD solution of $[Ru(terpy)(en)(H_2O)]^{2+}$ under an argon atmosphere. The final concentrations were as follows: 6.4×10^{-3} M Ru(II), 0.26 M $NaBH_4$, and D_2O/CD_3OD (1:9, v/v). A ^{1}H NMR spectrum was recorded approximately 3 min after the reaction was initiated. In parallel, the same mixture was prepared for a spectrophotometric experiment. To record an UV−vis spectrum of the $[Ru(terpy)(en)(H)]^+$ complex, a few drops of the reaction mixture were introduced to a cuvette filled with an argon-purged H_2O/EtOH solution (1:9, v/v).

RESULTS AND DISCUSSION

1. Preliminary Results. *a. Reaction of the Ru(II) Complex with $NaBH_4$ to Form the Corresponding Hydrido Complex.* Recently, experimental work in our laboratories showed that $[Ru^{II}(terpy)(en)H]^+$ can be formed directly in situ in the reaction of $[Ru^{II}(terpy)(en)(H_2O/EtOH)]^{2+}$ with $NaBH_4$. It is a relatively fast process, as can be seen in Figure 1, and the

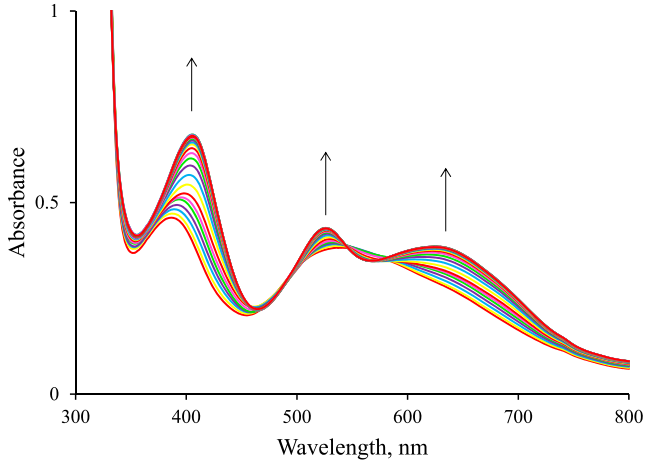

Figure 1. Spectral changes observed for the formation of $[Ru(terpy)(en)H]^+$ in a H_2O/EtOH (1:9, v/v) solution. Experimental conditions: $[Ru(II)] = 9.6 \times 10^{-5}$ M, $[BH_4^-] = 3.8 \times 10^{-3}$ M, argon atmosphere, T = 25 °C, l = 1 cm, and spectra recorded every 200 s.

hydrido complex is fairly stable in solution. Formation of the hydrido complex is accompanied by an increase in the absorbance intensity at both longer and shorter wavelengths, with isosbestic points at ca. 500, 547, and 577 nm. The absorption spectrum of the $[Ru^{II}(terpy)(en)H]^+$ complex exhibits bands at 404, 529, and 622 nm (Figure 1).

In order to gain further evidence for the formation of $[Ru(terpy)(en)H]^+$, ^{1}H NMR spectra were recorded for a much higher complex concentration in a large excess of $NaBH_4$, as reported in Figure S1. A characteristic hydride signal was observed at −1.58 ppm along with a multiplet for BH_4^- at ca. −5.0 ppm. These results are close to those reported for the $[Ru(tepy)(bipy)H]^+$ complex at −14.66 ppm.[39] Dilution of the sample used to record the ^{1}H NMR spectrum produced a characteristic UV−vis spectrum very close to that found for the final spectrum shown in Figure 1 (Figure S2).

Following formation of the hydride complex, we checked whether it can react with CO_2 to form the corresponding formato complex, Ru^{II}-OOCH. CO_2 gas was passed through the reaction mixture containing the hydrido complex Ru^{II}-H^-, as

https://dx.doi.org/10.1021/acs.inorgchem.0c01613
Inorg. Chem. 2020, 59, 14944−14953

was done before for the related $[Ru(tepy)(bipy)H]^+$ complex.[39] We observed a sudden hypsochromic shift characteristic for formation of the formato complex (Figure 2). These preliminary studies showed that it is possible to obtain the ruthenium(II) formato complex from the corresponding hydrido complex.

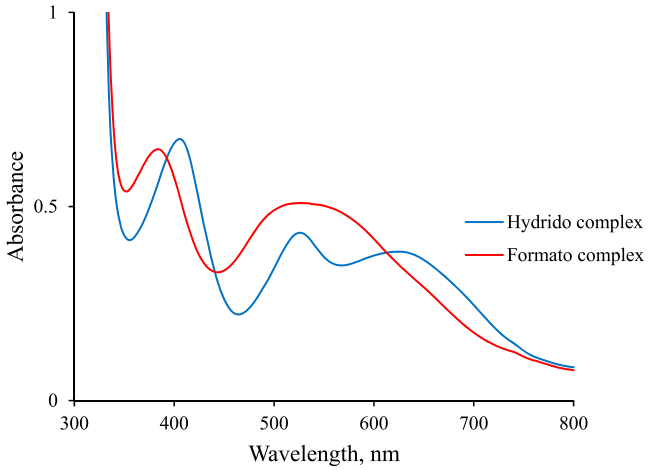

Figure 2. Comparison of the spectrum of $[Ru(terpy)(en)H]^+$ with that of the formato complex $[Ru(terpy)(en)(HCOO)]^+$ obtained in the reaction of $[Ru(terpy)(en)H]^+$ with CO_2 in a H_2O/EtOH (1:9, v/v) solution. Experimental conditions: $[Ru(II)] = 9.6 \times 10^{-5}$ M, $T = 25$ °C, and $l = 1$ cm.

b. Reaction of NAD^+ with $NaBH_4$ to Form NADH. It was furthermore demonstrated that, in the presence of an excess of BH_4^-, hydride is transferred to NAD^+, which is manifested by distinct spectral changes and the formation of a band at 340 nm, characteristic for NADH. The absorbance−time traces showed clean first-order kinetics (Figure S3). The observed rate constants are a linear function of the $NaBH_4$ concentration for the studied reaction, viz., $k_{obs} = k[BH_4^-]$ (Figure S4), where k represents the second-order rate constant for the reduction of NAD^+ by BH_4^- and equals $(1.23 \pm 0.03) \times 10^3$ M^{-1} s^{-1} at 15.2 °C. Note that this reaction is very fast, on a time scale of a few seconds (see further discussion).

c. Reaction of $[Ru^{II}(terpy)(en)(H_2O/EtOH)]^{2+}$ with NAD^+ in the Presence of Formate. Further preliminary experiments showed that a solvent composition of 1:9 (v/v) H_2O/EtOH seemed to work very well to reduce the reaction time for catalytic hydride transfer from NAD^+ to NADH in the presence of formate. Clear evidence for the formation of NADH similar to that shown in Figure S3 was observed. However, the observed reactions were extremely slow even at 36.8 °C and, under some experimental conditions, took 24 h, or even up to several days, to go to completion. The effect of the pH and buffers on the overall reaction was also studied. Depending on the formate concentration, the pH of the solution varied between 7.8 and 8.3, which is significantly far away from the pK_a value of the $[Ru(terpy)(en)(H_2O)]^{2+}$ complex, viz., $pK_a = 10.8$,[38] such that the hydroxo complex will not play any role during the reaction. The reactions were also studied in MES ($pK_a = 6.2$) and TRIS ($pK_a = 8.1$) at pH 7.1 and 7.4, respectively. The results for the reaction in a MES buffer are reported in Figure S5. The observed reaction rate of $(1.72 \pm 0.01) \times 10^{-5}$ M h^{-1} is very close to the limiting value found for the reaction under the selected conditions (see further discussion). However, in the case of the TRIS buffer (Figure S6), the reaction was found to be much slower, apparently because of the large fraction of H^+TRIS present in solution at the selected pH. This slowed the catalytic effect probably because of interaction of the protonated buffer with the $[Ru(terpy)(en)H]^+$ complex to form H_2. On the basis of these results, no buffers were employed in the subsequent work.

Two important blank experiments were performed to reveal the nature of the overall catalytic process. In the first experiment, spectral changes were monitored for the reaction between NAD^+ and $[Ru(terpy)(en)(H_2O/EtOH)]^{2+}$ in the absence of formate in a H_2O/EtOH (1:9, v/v) solution, which showed no formation of NADH (Figure S7). In the second experiment, spectral changes were monitored for the reaction between NAD^+ and formate in the absence of $[Ru(terpy)(en)(H_2O/EtOH)]^{2+}$ in the same solvent, which again showed no formation of NADH (Figure S8). The results demonstrate that both formate and $[Ru(terpy)(en)(H_2O/EtOH)]^{2+}$ are required to convert NAD^+ to NADH. Furthermore, it also demonstrates that the selected solvent is not a source of hydride in these reactions.

On the basis of these preliminary results, we report on a hydride transfer reaction in the presence of formate for the conversion of NAD^+ to NADH catalyzed by the ruthenium(II) polypyridylamine complex $[Ru^{II}(terpy)(en)(H_2O/EtOH)]^{2+}$.

2. Reactions of the Ru(II) Complex with Formate, Acetate, and Chloride. We started our studies with reactions of $[Ru^{II}(terpy)(en)(H_2O/EtOH)]^{2+}$ with formate and acetate in a H_2O/EtOH (1:9, v/v) solution as a comparison to earlier studies of the complex with chloride.[38] Characteristic spectral changes are shown in Figure 3, from which it follows that clean and very similar isosbestic points are observed for both nucleophiles, and the kinetic traces follow a single-exponential function. Plots of k_{obs} versus formate and acetate concentrations show saturation kinetics with a significant intercept, as reported in parts a and b of Figure 4, respectively. The following reaction mechanism is suggested to account for the observed kinetic data (eq 1):

$$[Ru^{II}(terpy)(en)(H_2O/EtOH)]^{2+} + RCOO^- \rightleftharpoons \{[Ru^{II}(terpy)(en)(H_2O/EtOH)]^{2+} \cdot RCOO^-\} \quad Q_1$$
$$k_{-1} \Vert k_1$$
$$[Ru^{II}(terpy)(en)(RCOO)]^+ + H_2O/EtOH \quad (1)$$

where Q_1 is the precursor (ion-pair) formation constant and k_1 and k_{-1} are the forward and backward rate constants, respectively. The observed rate constant for the suggested mechanism presented in eq 1 is given by eq 2:

$$k_{obs} = k_{-1} + \frac{k_1 Q_1 [RCOO^-]}{1 + Q_1 [RCOO^-]} \quad (2)$$

The overall equilibrium constant is given by eq 3.

$$K = \frac{k_1 Q_1}{k_{-1}} \quad (3)$$

Both formate and acetate show a very similar behavior in an aqueous EtOH solution but totally different from that found for chloride as the entering nucleophile in H_2O as the solvent at 25 °C.[38] In the latter case, a linear correlation between k_{obs} and $[Cl^-]$ was found with a slope of $(1.28 \pm 0.04) \times 10^{-2}$ M^{-1} s^{-1} (for the forward reaction) and intercept of $(7.9 \pm 0.6) \times 10^{-3}$ s^{-1} (for the backward reaction) to give an overall equilibrium constant of 1.6 ± 0.2 M^{-1} at 25 °C for the anation reaction by chloride. These measurements were here repeated because of the totally different reaction medium and temperature used in

https://dx.doi.org/10.1021/acs.inorgchem.0c01613
Inorg. Chem. 2020, 59, 14944−14953

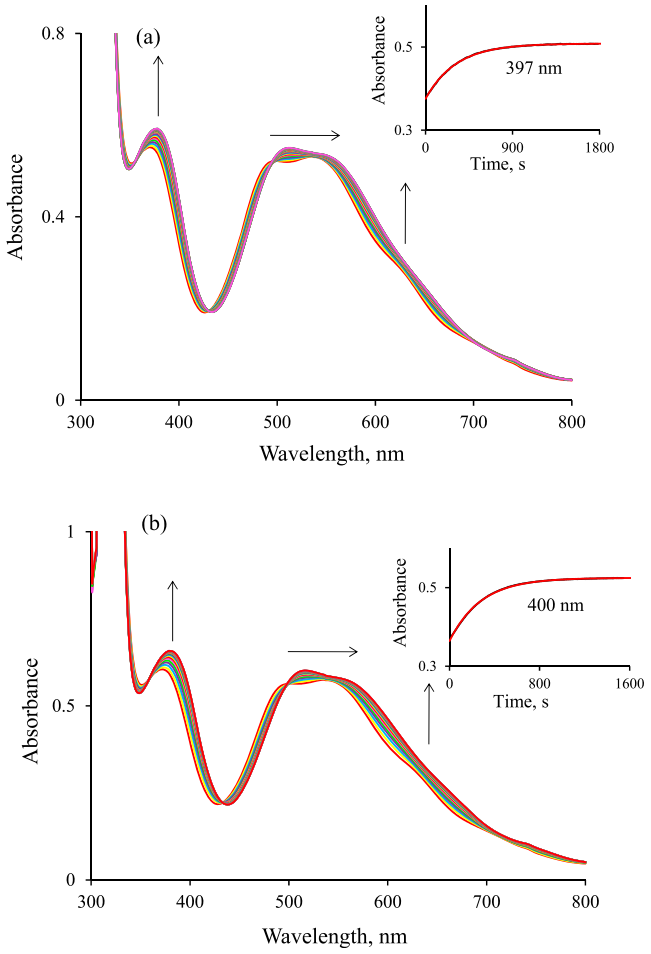

Figure 3. Spectral changes observed during the anation of $[Ru^{II}(terpy)(en)(H_2O/EtOH)]^{2+}$ by (a) formate and (b) acetate in a H_2O/EtOH (1:9, v/v) solution. Experimental conditions: [Ru(II)] = 10.6×10^{-5} M, $[RCOO^-] = 1.12 \times 10^{-4}$ M, T = 36.8 °C, and spectra recorded every (a) 60 and (b) 65 s.

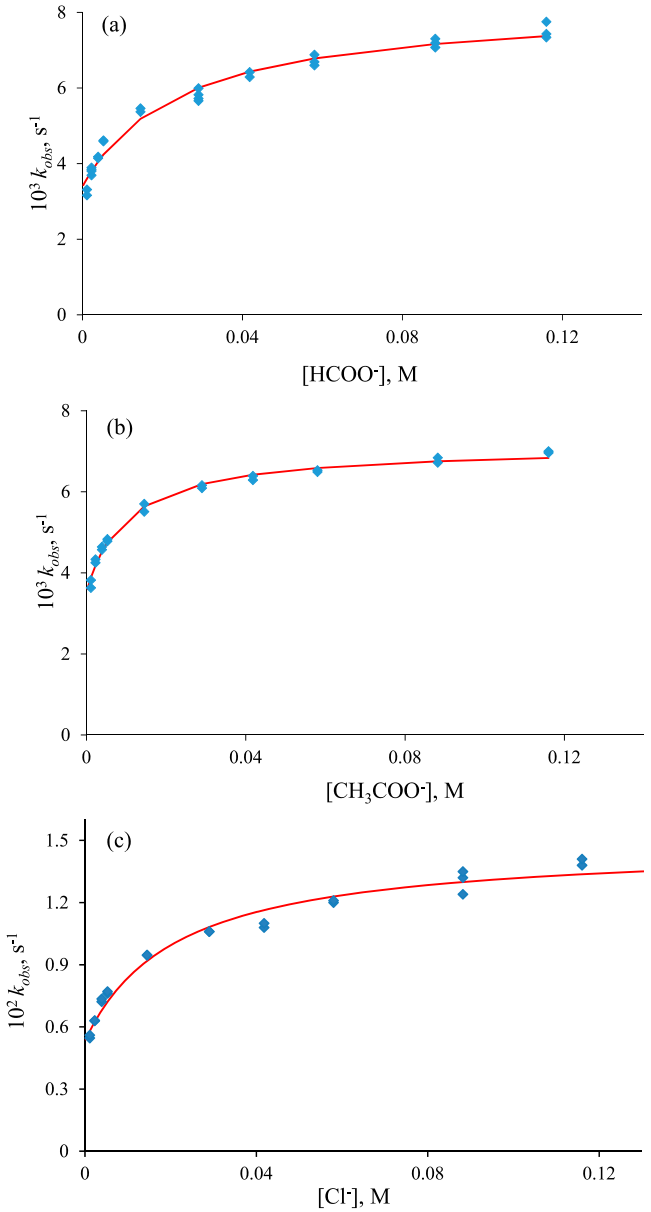

Figure 4. Dependence of k_{obs} on (a) $[HCOO^-]$, (b) $[CH_3COO^-]$, and (c) $[Cl^-]$ for the anation of $[Ru^{II}(terpy)(en)(H_2O/EtOH)]^{2+}$ in a H_2O/EtOH (1:9, v/v) solution. Experimental conditions: [Ru(II)] = 10.6×10^{-5} M and T = 36.8 °C.

the present study, viz., 1:9 (v/v) H_2O/EtOH and 36.8 °C. For formate, acetate, and chloride as entering nucleophiles, the initial slopes of the plots in Figure 4 are given by k_1Q_1, i.e., the second-order rate constant, such that the overall equilibrium constant is given by $K = k_1Q_1/k_{-1}$. The results obtained for all three nucleophiles are summarized in Table 1. The data indicate that all of the reactions are quite fast and go to completion on a time scale of between 8 and 17 min for formate as the entering ligand at concentrations within the range applied for the catalytic hydride transfer studies. This is an important observation in terms of the subsequent reactions studied in the presence of NAD^+. The reactions with chloride are ca. 2−3 times faster than those with formate and acetate on the basis of the k_1Q_1 values in Table 1. The overall equilibrium constants (K) follow the sequence chloride > acetate > formate in a 1:9 (v/v) H_2O/EtOH solvent mixture. The value of K for the formation of $[Ru^{II}(terpy)(en)(HCOO)]^+$ is such that, for the lowest formate concentration of 1 mM, ca. 5% of the total Ru(II) complex will be in the formato form, whereas at the highest formate concentration of 0.12 M, ca. 87% will be present in the formato form. This accounts for the saturation reached at high formate concentrations in Figure 4a. The ion-pair formation constants (Q_1) follow the sequence acetate > chloride > formate and are rather high as a result of the relatively low polarity of the reaction medium. In the case of acetate and formate, the trend in Q_1 is in line with the inductive effect of the methyl group, which increases the electron density on the carboxylate group and

Table 1. Summary of the Rate and Equilibrium Constants for the Anation of $[Ru^{II}(terpy)(en)(H_2O/EtOH)]^{2+}$ by Formate, Acetate, and Chloride in a H_2O/EtOH (1:9, v/v) Solution at 36.8 °C

	entering ligand		
constant	formate	acetate	chloride
$10^3 k_1$, s^{-1}	4.8 ± 0.2	3.60 ± 0.09	9.5 ± 0.4
Q_1, M^{-1}	41 ± 7	98 ± 13	68 ± 2
k_1Q_1, M^{-1} s^{-1}	0.20 ± 0.04	0.35 ± 0.05	0.65 ± 0.05
$10^3 k_{-1}$, s^{-1}	3.4 ± 0.1	3.5 ± 0.1	4.7 ± 0.3
$K = k_1Q_1/k_{-1}$, M^{-1}	59 ± 13	100 ± 17	138 ± 19

https://dx.doi.org/10.1021/acs.inorgchem.0c01613
Inorg. Chem. 2020, 59, 14944−14953

correlates with the difference in basicity, as expressed by the pK_a values for acetic acid (4.7) and formic acid (3.7), respectively. Aquation/solvolysis of the formed complexes (k_{-1}) occurs on approximately the same time scale, which in the case of the chloride complex, used as the starting material in the subsequent studies, takes ca. 12 min prior to mixing the reactants at 36.8 °C. The slightly faster aquation of the latter complex may be related to the significantly larger ionic radius of Cl^- (181 pm) compared to that of $HCOO^-$ (136 pm) in terms of a less concentrated negative charge on Cl^- than on $HCOO^-$.[40,41]

3. Kinetic Data for Reaction of the Ru(II) Complex with Formate as the Source of Hydride for the Conversion of NAD^+ to NADH. Some very interesting observations were made for the reactions observed in the $[Ru^{II}(terpy)(en)(H_2O/EtOH)]^{2+}$–formate–$NAD^+$ system. In the presence of a large excess of formate, the reaction showed a typical zero-order formation of NADH with a characteristic dead end, as shown in Figure 5a. At a much lower formate concentration, a typical pseudo-first-order kinetic trace was obtained that could be fitted with a single-exponential function, as presented in Figure 5b.

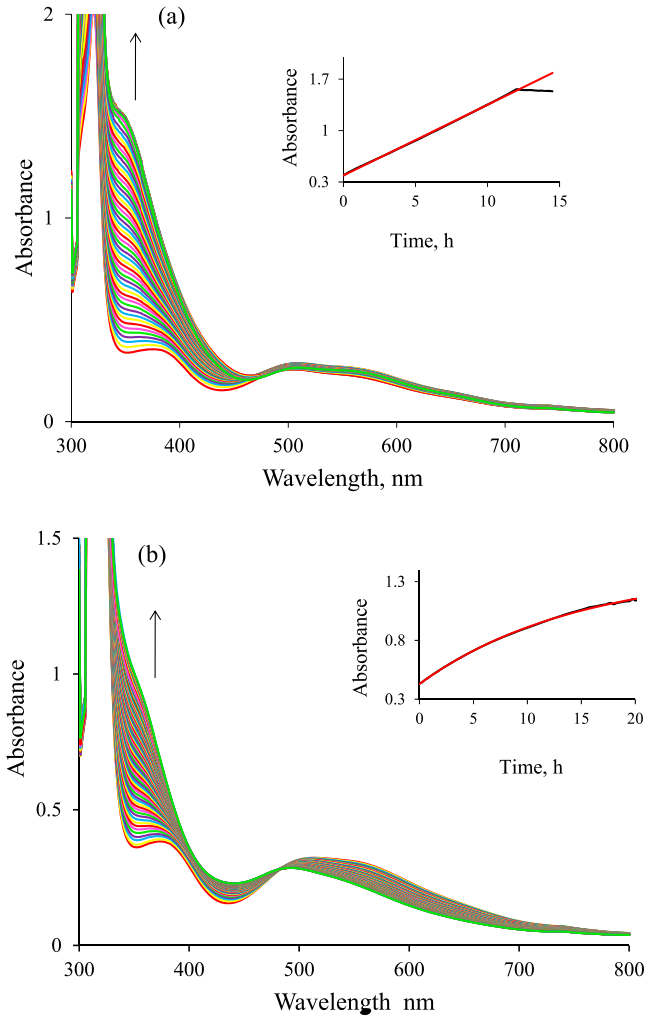

Figure 5. Spectral changes observed during the catalyzed reduction of NAD^+ to 1,4-NADH in the presence of formate in a H_2O/EtOH (1:9 v/v) solution. Experimental conditions: (a) $[HCOO^-]$ = 0.0145 M, (b), $[HCOO^-]$ = 0.0011 M; [Ru] = 5.3×10^{-5} M, $[NAD^+] = 3.1 \times 10^{-4}$ M, T = 36.8 °C, and spectra recorded every 15 min. Insets: Kinetic traces recorded at 340 nm.

Under the applied conditions, the reaction of the Ru(II) complex with formate (vide supra) is orders of magnitude faster than the formation of NADH monitored at 340 nm, indicating that a subsequent reaction step must be rate-determining! In general, all kinetic data obtained at $[HCOO^-] < 1.65 \times 10^{-3}$ M showed first-order behavior, and k_{obs} was independent of the formate concentration with an average value of $(6.48 \pm 0.02) \times 10^{-2}$ h^{-1} at a Ru(II) complex concentration of 5.3×10^{-5} M and 36.8 °C. At $[HCOO^-] > 2.2 \times 10^{-3}$ M, all kinetic traces showed zero-order behavior of which the slope represents the zero-order rate constant.

A summary of all kinetic data measured as a function of the formate concentration is given in Table S1. A plot of the initial rate and zero-order rate constant for kinetic traces that follow first- and zero-order kinetics, respectively, as a function of $[HCOO^-]$, is presented in Figure 6.

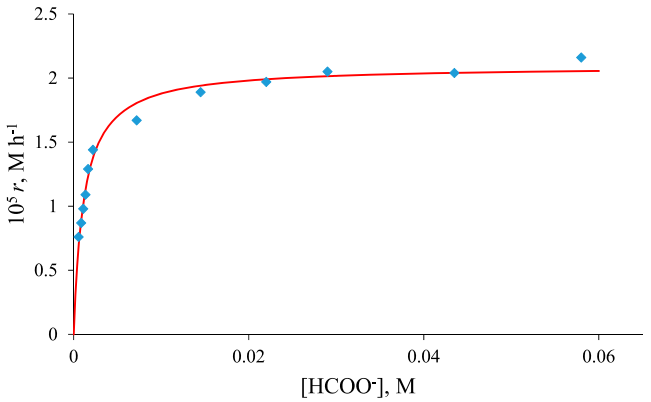

Figure 6. Dependence of the initial rate (for the first-order reactions, followed at low formate concentrations) or zero-order rate constant (for the zero-order reactions at higher formate concentrations) on $[HCOO^-]$ for the catalyzed reduction of NAD^+ to 1,4-NADH in a H_2O/EtOH (1:9, v/v) solution. Experimental conditions: [Ru(II)] = 5.3×10^{-5} M, $[NAD^+] = 3.1 \times 10^{-4}$ M, T = 36.8 °C; r = initial or zero-order rate constant with increasing formate concentration; $k_2 = (2.09 \pm 0.04) \times 10^{-5}$ M h^{-1} and $Q_2 = 869 \pm 63$ M^{-1} (see eq 6).

Figure 6 suggests that, following the rapid and reversible formation of the $[Ru^{II}(terpy)(en)(HCOO)]^+$ complex that depends on the formate concentration as described in the previous section, formate apparently plays a further catalytic role and controls the rate of the subsequent hydride transfer process. To account for this effect, we suggest the following reaction mechanism outlined in eq 4, followed by the fast reaction in eq 5:

$$[Ru^{II}(terpy)(en)(HCOO)]^+ + HCOO^- \overset{Q_2}{\rightleftharpoons} \{[Ru^{II}(terpy)(en)(HCOO)]^+ \cdot HCOO^-\}$$
$$\downarrow k_2$$
$$[Ru^{II}(terpy)(en)(H)]^+ + HCOO^- + CO_2 \quad (4)$$

$$[Ru^{II}(terpy)(en)(H)]^+ + NAD^+ \xrightarrow[+H_2O/EtOH]{fast} [Ru^{II}(terpy)(en)(H_2O/EtOH)]^{2+} + NADH \quad (5)$$

In this mechanism, the rate-determining step involves the formate-catalyzed rearrangement of coordinated formate from the O,O bonding mode of formate to the O,H bonding mode,[23] coupled with the release of CO_2 and formation of the hydride complex, which subsequently reacts rapidly with NAD^+ to form NADH, as shown in our preliminary experiments. This

https://dx.doi.org/10.1021/acs.inorgchem.0c01613
Inorg. Chem. 2020, 59, 14944–14953

suggestion is based on the linkage isomerization mechanism recently suggested by Sadler et al. based on computational density functional theory (DFT) calculations.[23] Our suggested mechanism is based on a formate−CO_2 adduct is released. Furthermore, hydride in the form of Ru^{II}-H^- can rapidly react with NAD^+ to form NADH in a non-rate-determining step.

The rate of the reaction step between Ru^{II}-H^- and NAD^+ to form NADH is orders of magnitude faster than decarboxylation of the ruthenium(II) formato complex to form the ruthenium-(II) hydrido complex, as illustrated by our preliminary measurements for the conversion of NAD^+ to NADH with BH_4^- as the source of hydride. Thus, the actual rearrangement of the formato complex to the hydrido complex is suggested to be the rate-determining step of the overall process, which is catalyzed by formate.

The experimental data in Figure 6 were fitted to eq 6:

$$r = \frac{\mathrm{d[NADH]}}{\mathrm{d}t} = \frac{k_2 Q_2 [\mathrm{HCOO^-}]}{1 + Q_2[\mathrm{HCOO^-}]} \tag{6}$$

where Q_2 represents the precursor formation of the catalytic intermediate and k_2 the limiting rate reached at a high formate concentration. The fit of the data in Figure 6 results in $k_2 = (2.09 \pm 0.04) \times 10^{-5}$ M h^{-1} and $Q_2 = 869 \pm 63$ M^{-1} at 36.8 °C. At low formate concentration, the rate law simplifies to eq 7

$$r = \frac{\mathrm{d[NADH]}}{\mathrm{d}t} = k_2 Q_2 [\mathrm{HCOO^-}] \tag{7}$$

such that the initial slope of the plot in Figure 6 is represented by $k_2Q_2 = (1.8 \pm 0.2) \times 10^{-2}$ h^{-1}. At a high formate concentration, the rate law in eq 6 simplifies to eq 8

$$r = \frac{\mathrm{d[NADH]}}{\mathrm{d}t} = k_2 \tag{8}$$

and reaches a limiting zero-order rate constant of $k_2 = (2.09 \pm 0.04) \times 10^{-5}$ M h^{-1}. The value of Q_2 controls the fraction of the Ru(II) complex in the form of a catalytic intermediate, which varies between 0.30 and 0.98 over the formate concentration range employed. The changeover from first- to zero-order kinetics occurs at a total formate concentration of 2.2 mM. At this point, the mole fraction of the catalytic intermediate based on the value of Q_2 is 0.65 and increases drastically to 0.86 at a formate concentration of 7 mM. This sudden increase is suggested to account for the changeover in the kinetic behavior from first- to zero-order kinetics with increasing formate concentration.

4. Kinetic Data for the Formation of NADH as a Function of the Ru(II) Concentration in the Presence of Formate. The Ru(II) complex concentration was varied at both fixed low and high formate concentrations, i.e., where the reaction shows typical first- and zero-order behavior, respectively. The results summarized in Figure 7 indicate that at low formate concentration the first-order rate constant shows saturation kinetics, whereas at high formate concentration, the zero-order rate constant shows a linear dependence on the Ru(II) concentration. The empirical rate law suggested to account for the kinetic results reported in Figure 7a is as follows:

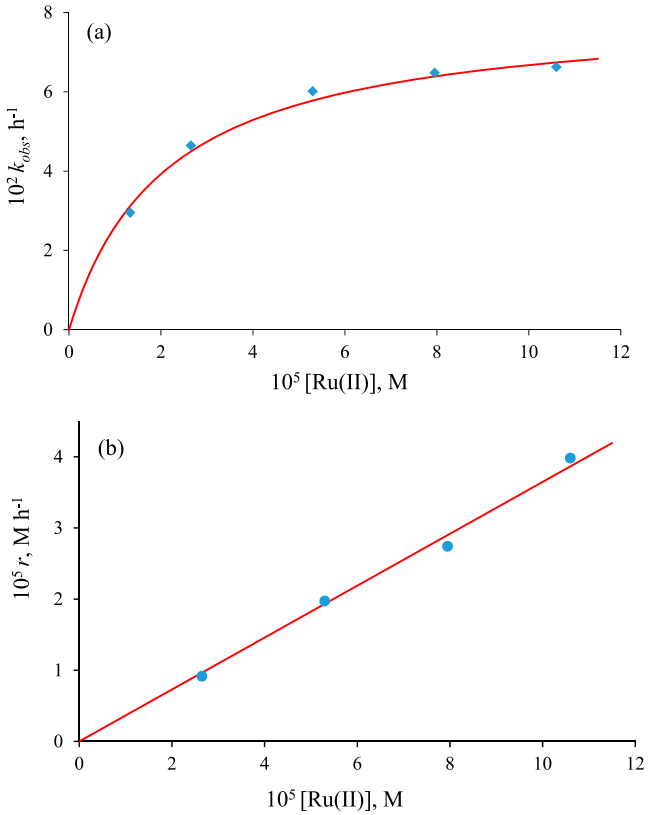

Figure 7. Dependence of (a) k_{obs} and (b) the rate on [Ru(II)] for the reduction of NAD^+ to 1,4-NADH in the presence of formate in a H_2O/EtOH (1:9, v/v) solution. Experimental conditions: $[NAD^+] = 3.1 \times 10^{-4}$ M; $T = 36.8$ °C; (a) $[HCOO^-] = 0.0011$ M; $k_2'k_3Q_3 = (3.8 \pm 0.6) \times 10^3$ M^{-1} h^{-1}; $k_2'k_3 = (8.1 \pm 0.3) \times 10^{-2}$ h^{-1} (see eqs 13 and 14); (b) $[HCOO^-] = 0.022$ M; $k_2''k_3Q_3 = 0.36 \pm 0.01$ h^{-1} (see eq 18).

$$r = \frac{\mathrm{d[NADH]}}{\mathrm{d}t} = -\frac{\mathrm{d[NAD^+]}}{\mathrm{d}t} = \frac{k_2 k_3 Q_2 Q_3 [\mathrm{HCOO^-}][\mathrm{Ru(II)}]}{(1 + Q_2[\mathrm{HCOO^-}])(1 + Q_3[\mathrm{Ru(II)}])}[\mathrm{NAD^+}] \tag{9}$$

where

$$k_{obs} = \frac{k_2 k_3 Q_2 Q_3 [\mathrm{HCOO^-}][\mathrm{Ru(II)}]}{(1 + Q_2[\mathrm{HCOO^-}])(1 + Q_3[\mathrm{Ru(II)}])} \tag{10}$$

Q_3 represents the precursor formation constant for the equilibrium between the Ru(II) complex and NAD^+ to account for the nonlinear Ru(II) concentration dependence reported in Figure 7a.

For a particular formate concentration, the rate expression in eq 10 simplifies to eq 11

$$k_{obs} = \frac{k_2' k_3 Q_3 [\mathrm{Ru(II)}]}{1 + Q_3[\mathrm{Ru(II)}]} \tag{11}$$

where

$$k_2' = \frac{k_2 Q_2 [\mathrm{HCOO^-}]}{1 + Q_2[\mathrm{HCOO^-}]} \tag{12}$$

At low [Ru(II)], eq 11 simplifies to eq 13

$$k_{obs} = k_2' k_3 Q_3 [\mathrm{Ru(II)}] \tag{13}$$

https://dx.doi.org/10.1021/acs.inorgchem.0c01613
Inorg. Chem. 2020, 59, 14944−14953

whereas at high [Ru(II)], eq 11 simplifies to eq 14

$$k_{obs} = k_2'k_3 \quad (14)$$

where [Ru(II)] represents $[Ru^{II}(terpy)(en)(HCOO)]^+$. These rate expressions are in line with the saturation effect observed in Figure 7a, for which the initial slope $k_2'k_3Q_3 = (3.8 \pm 0.6) \times 10^3$ M^{-1} h^{-1} and the limiting rate constant $k_2'k_3 = (8.1 \pm 0.3) \times 10^{-2}$ h^{-1}.

In the case of the higher formate concentration under which zero-order kinetics was observed, the results in Figure 7b show a linear dependence on the Ru(II) concentration. Under these conditions, the rate expression is given by eq 15:

$$r = \frac{d[NADH]}{dt} = \frac{k_2k_3Q_2Q_3[HCOO^-][Ru(II)]}{(1 + Q_2[HCOO^-])(1 + Q_3[Ru(II)])} \quad (15)$$

which, at a particular formate concentration, simplifies to eq 16 with k_2'' defined in eq 17:

$$r = \frac{d[NADH]}{dt} = \frac{k_2''k_3Q_3[Ru(II)]}{1 + Q_3[Ru(II)]} \quad (16)$$

$$k_2'' = \frac{k_2Q_2[HCOO^-]}{1 + Q_2[HCOO^-]} \quad (17)$$

For the linear concentration dependence presented in Figure 7b, eq 16 reduces to eq 18:

$$r = \frac{d[NADH]}{dt} = k_2''k_3Q_3[Ru(II)] \quad (18)$$

for which $k_2''k_3Q_3 = 0.36 \pm 0.01$ h^{-1} at 36.8 °C.

5. Kinetic Data as a Function of [NAD$^+$]. Kinetic experiments were performed as a function of the NAD^+ concentration at low and high formate concentrations, as summarized in Table 2. The absorbance change (ΔA) as a function of the NAD^+ concentration is shown in Figure 8 for low and high formate concentrations. The results summarized in Table 2 indicate that both the observed first- and zero-order rate constants at low and high formate concentrations, respectively, are independent of $[NAD^+]$. Furthermore, the results shown in Figure 8 clearly indicate that the NAD^+ concentration does not affect the absorbance change during the first-order kinetics at low formate concentration, but at higher formate concentration where zero-order kinetics are observed, the absorbance change increases with increasing NAD^+ concentration, however, with the same zero-order rate constant. Thus, NAD^+ is converted to NADH independent of the NAD^+ concentration. This means that NAD^+ is not part of the rate-determining step, which is in line with our mechanistic understanding of the two-step reaction mechanism (see further discussion).

Table 2. First- and Zero-Order Rate Constants Measured at Low and High Formate Concentrations as a Function of the NAD$^+$ Concentration for the Catalyzed Reduction of NAD$^+$ to 1,4-NADH[a]

	[HCOO$^-$], M	
	0.0011	0.022
10^4[NAD$^+$], M	10^2k_{obs}, h^{-1}	10^5r, M h^{-1}
0.5		2.21 ± 0.03
1.0		1.85 ± 0.02
1.5	6.62 ± 0.02	
2.0	6.19 ± 0.07	1.87 ± 0.01
3.1	6.80 ± 0.09	1.97 ± 0.01
4.0	5.44 ± 0.07	

[a]Experimental conditions: [Ru(II)] = 5.3×10^{-5} M, T = 36.8 °C, and a H_2O/EtOH (1:9, v/v) solution.

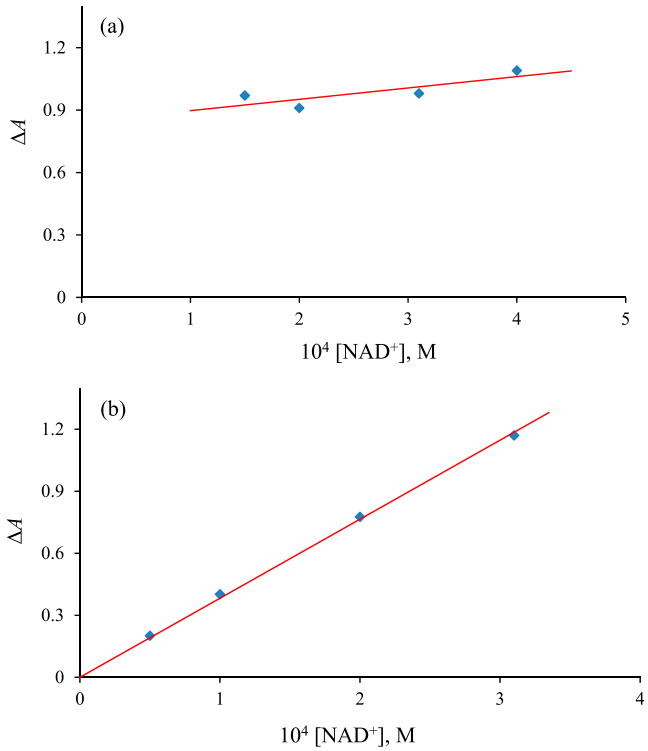

Figure 8. Dependence of the absorbance increase (ΔA) on $[NAD^+]$ for the catalyzed reduction reaction of NAD^+ to 1,4-NADH in the presence of formate in a H_2O/EtOH (1:9, v/v) solution. Experimental conditions: (a) $[HCOO^-]$ = 0.0011 M, (b) $[HCOO^-]$ = 0.022 M; [Ru(II)] = 5.3×10^{-5} M; T = 36.8 °C.

A reviewer kindly suggested that we should measure the kinetic isotope effect (KIE) for deuterated sodium formate because that should show the crucial role of formation of the Ru-H^- complex in the catalytic cycle. A typical kinetic trace for the reaction with deuterated sodium formate is shown in Figure 9. The observed reaction rate was found to be $(0.81 \pm 0.01) \times 10^{-5}$ M h^{-1} at 36.8 °C. A duplicate experiment showed a reaction rate of $(0.90 \pm 0.02) \times 10^{-5}$ M h^{-1}; thus, an average value of $(0.86 \pm 0.08) \times 10^{-5}$ M h^{-1} was found, compared to $(2.05 \pm 0.01) \times 10^{-5}$ M h^{-1} measured for normal sodium formate (see Figure 6). This results in a KIE of 2.05/0.86 = 2.4. In a recent paper by Wang et al.[42] on the dehydrogenation of formic acid catalyzed by a bioinspired Ir(III) complex, a KIE of between 1.4 and 2.3 was reported, which is close to that found in the present study.

Finally, we studied the temperature dependence of the overall reaction rate at a high formate concentration selected from Figure 6 to determine the activation parameters in order to reveal further mechanistic information. The results are reported in Figure S9 and Table S2, from which $\Delta H^‡$ and $\Delta S^‡$ have the values 82 ± 3 kJ mol^{-1} and −139 ± 8 J mol^{-1} K^{-1}, respectively, based on the reaction rate data, i.e., the zero-order rate constant. Table S2 also contains the activation parameters for the converted first- and second-order rate constants. The values of $\Delta H^‡$ remain constant for all three rate constants, but the values of $\Delta S^‡$ become more positive because of their increase in

https://dx.doi.org/10.1021/acs.inorgchem.0c01613
Inorg. Chem. 2020, 59, 14944−14953

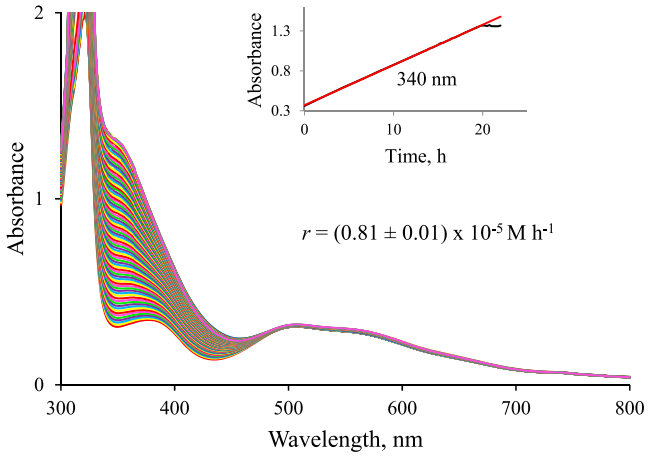

Figure 9. Spectral changes observed during the catalyzed reduction of NAD^+ to 1,4-NADH in the presence of deuterated formate in a H_2O/EtOH (1:9, v/v) solution. Experimental conditions: $[DCOO^-] = 0.029$ M, $[Ru] = 5.3 \times 10^{-5}$ M, $[NAD^+] = 3.1 \times 10^{-4}$ M, $T = 36.8$ °C, and spectra recorded every 15 min. Inset: Kinetic traces recorded at 340 nm.

absolute number. All in all, the rate-determining step of the reaction is characterized by a very negative activation entropy (see further discussion).

6. Kinetic Data as a Function of the Solvent Composition. Upon a change of the solvent composition from 1:9 to 5:5 (v/v) H_2O/EtOH, the observed reaction slowed considerably and changed from a zero-order to a first-order process in the presence of a high formate concentration (Table 3). These results demonstrate that increasing the H_2O concentration to ca. 50% decreases the reaction rate by approximately a factor of 4. This must be associated with the increase in the polarity of the solvent upon going to higher H_2O concentrations (the dielectric constant for EtOH is 24.3 compared to 78.4 for H_2O).[43] For the 1:9 (v/v) H_2O/EtOH solvent mixture used in most of the reported work, the polarity of the solvent is expected to be low, which will support ion-pair formation, i.e., formation of the catalytic intermediate ion-pair complex (see eq 4), which accelerates the overall catalytic process.

Table 3. Kinetic Data for the Catalyzed Reduction of NAD^+ to 1,4-NADH in the Presence of Formate in a H_2O/EtOH Medium of Varying Composition[a]

H_2O/EtOH (v/v)	$10^5 r$, M h^{-1}	$10^2 k_{obs}$, h^{-1}	$10^5 r$,[b] M h^{-1}
1:9	1.97 ± 0.01		
3:7	1.10 ± 0.01		
5:5		2.2 ± 0.1	0.49 ± 0.06

[a]Experimental conditions: $[Ru(II)] = 5.3 \times 10^{-5}$ M, $[HCOO^-] = 0.0435$ M, $[NAD^+] = 3.1 \times 10^{-4}$ M, and $T = 36.8$ °C. [b]Initial rate.

7. Reaction Mechanism Proposed on the Basis of the Reported Kinetic Data. On the basis of the reported kinetic results, we suggest the reaction mechanism presented in Scheme 1, which can account for all of the observed kinetic trends.

The reaction cycle starts with reaction ①, during which the Ru^{II}-solv complex is rapidly converted reversibly to the formato complex Ru^{II}-OC(O)H in a clockwise direction. In reaction ②, the formato complex undergoes a partial hydride ring-closure reaction from an end-on-bonded to an O,H-bonded chelate to form the Ru^{II}-O(H)CO complex, as suggested by Sadler et al. based on DFT calculations.[23] For the subsequent slow reaction ③, we found evidence for formate-catalyzed decarboxylation (Figure 6) to form the Ru^{II}-(H) hydrido complex under the release of formate and CO_2, which is the rate-determining step ④ of the catalytic cycle. The hydrido complex formed reacts rapidly with NAD^+ to produce NADH and to regenerate Ru^{II}-solv in step ⑤, by which the catalytic cycle is completed. The KIE of 2.4 can be accounted for in terms of cleavage of the C−H bond during formation of the Ru^{II}-(H) hydrido complex in the rate-determining step ④. The very negative activation entropy of -139 ± 8 J mol^{-1} K^{-1} found for the rate-determining step ④ could be associated with a highly structured transition state that involves the formate-catalyzed decarboxylation reaction to form the Ru^{II}-(H) hydrido complex.

■ ASSOCIATED CONTENT

Supporting Information

The Supporting Information is available free of charge at https://pubs.acs.org/doi/10.1021/acs.inorgchem.0c01613.

Figures S1−S8 reporting ^{1}H NMR spectra, UV−vis spectra of the hydrido complex, spectral changes observed during the reaction of NAD^+ with $NaBH_4$, dependence of k_{obs} on $[NaBH_4]$ for the reduction of NAD^+, spectral changes observed during the reaction of NAD^+ and $[Ru(terpy)(en)(H_2O/EtOH)]^+$ in the absence of formate, spectral changes observed during the reaction of NAD^+ and formate in the absence of $[Ru(terpy)(en)(H_2O/EtOH)]^+$, spectral changes observed during the catalyzed reduction of NAD^+ to 1,4-NADH in a MES buffer, and spectral changes observed during the catalyzed reduction of NAD^+ to 1,4-NADH in a TRIS buffer, and

Scheme 1. Proposed Reaction Scheme Based on the Obtained Kinetic Data, Where Solvent (solv) Represents the 1:9 (v/v) H_2O/EtOH Solvent Mixture

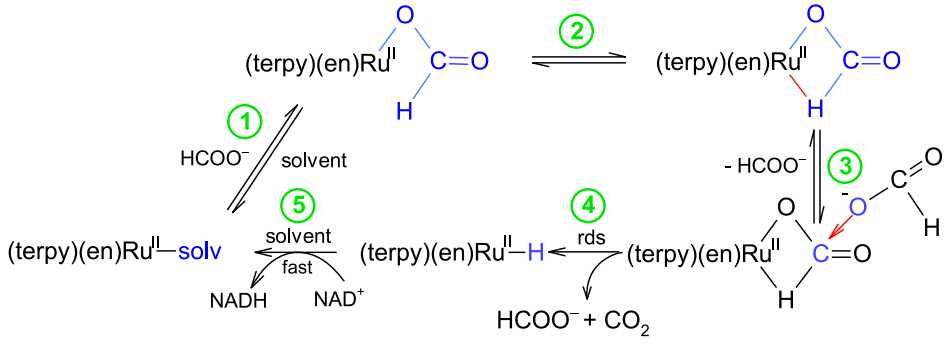

https://dx.doi.org/10.1021/acs.inorgchem.0c01613
Inorg. Chem. 2020, 59, 14944−14953

summaries of the kinetic data (Table S1) and temperature-dependent kinetic data (Table S2) (PDF)

AUTHOR INFORMATION

Corresponding Author

Rudi van Eldik − *Faculty of Chemistry, Nicolaus Copernicus University in Toruń, 87-100 Toruń, Poland; Department of Chemistry and Pharmacy, University of Erlangen-Nuremberg, 91058 Erlangen, Germany;* orcid.org/0000-0003-4271-0118; Email: rudi.vaneldik@fau.de

Authors

Marta Chrzanowska − *Faculty of Chemistry, Nicolaus Copernicus University in Toruń, 87-100 Toruń, Poland;* orcid.org/0000-0002-1725-3026

Anna Katafias − *Faculty of Chemistry, Nicolaus Copernicus University in Toruń, 87-100 Toruń, Poland;* orcid.org/0000-0001-5536-4280

Complete contact information is available at: https://pubs.acs.org/10.1021/acs.inorgchem.0c01613

Author Contributions

The synthetic work and kinetic measurements were performed by M.C. A.K. and R.v.E. developed the concept of the manuscript and accept responsibility for the reported work. All authors contributed equally to writing the manuscript.

Notes

The authors declare no competing financial interest.

ACKNOWLEDGMENTS

This project was supported financially by the National Science Center, Poland (Grant Preludium 2019/33/N/ST4/00700).

REFERENCES

(1) Armstrong, D., Stratton, R. D., Eds. *Oxidative Stress and Antioxidant Protection: The Science of Free Radical Biology and Disease*; John Wiley & Sons: Hoboken, NJ, 2012.

(2) Romero-Canelón, I.; Sadler, P. J. Next-Generation Metal Anticancer Complexes: Multitargeting via Redox Modulation. *Inorg. Chem.* **2013**, *52*, 12276−12291.

(3) Manda, G.; Isvoranu, G.; Comanescu, M. V.; Manea, A.; Debelec Butuner, B.; Korkmaz, K. S. The redox biology network in cancer pathophysiology and therapeutics. *Redox Biol.* **2015**, *5*, 347−357.

(4) Ye, Z. W.; Zhang, J.; Townsend, D. M.; Tew, K. D. Oxidative stress, redox regulation and diseases of cellular differentiation. *Biochim. Biophys. Acta, Gen. Subj.* **2015**, *1850*, 1607−1621.

(5) Pérez-Torres, I.; Guarner-Lans, V.; Rubio-Ruiz, M. E. Reductive stress in inflammation-associated diseases and the pro-oxidant effect of antioxidant agents. *Int. J. Mol. Sci.* **2017**, *18*, 2098.

(6) Xiao, W.; Wang, R.-S.; Handy, D. E.; Loscalzo, J. NAD(H) and NADP(H) redox couples and cellular energy metabolism. *Antioxid. Redox Signaling* **2018**, *28*, 251−272.

(7) Lee, B. W. L.; Ghode, P.; Ong, D. S. T. Redox regulation of cell state and fate. *Redox Biol.* **2019**, *25*, 101056.

(8) Zhang, L.; Wang, X.; Cueto, R.; Effi, C.; Zhang, Y.; Tan, H.; Qin, X.; Ji, Y.; Yang, X.; Wang, H. Biochemical basis and metabolic interplay of redox regulation. *Redox Biol.* **2019**, *26*, 101284.

(9) Xiao, W.; Loscalzo, J. Metabolic responses to reductive stress. *Antioxid. Redox Signaling* **2020**, *32*, 1330−1347.

(10) Batinic-Haberle, I.; Tovmasyan, A.; Spasojevic, I. An educational overview of the chemistry, biochemistry and therapeutic aspects of Mn porphyrins − From superoxide dismutation to H_2O_2-driven pathways. *Redox Biol.* **2015**, *5*, 43−65.

(11) Batinic-Haberle, I., Reboucas, J., Spasojevic, I., Eds. *Redox-active therapeutics. Oxidative stress in applied basic research and clinical practice*; Springer International Publishing: Cham, Switzerland, 2016.

(12) Chaiswing, L.; St. Clair, W. H.; St. Clair, D. K. Redox Paradox: A novel approach to therapeutics-resistant cancer. *Antioxid. Redox Signaling* **2018**, *29*, 1237−1272.

(13) Hegedüs, C.; Kovács, K.; Polgár, Z.; Regdon, Z.; Szabó, É.; Robaszkiewicz, A.; Forman, H. J.; Martner, A.; Virág, L. Redox control of cancer cell destruction. *Redox Biol.* **2018**, *16*, 59−74.

(14) Wang, K.; Jiang, J.; Lei, Y.; Zhou, S.; Wei, Y.; Huang, C. Targeting metabolic−redox circuits for cancer therapy. *Trends Biochem. Sci.* **2019**, *44*, 401−414.

(15) Privat-Maldonado, A.; Schmidt, A.; Lin, A.; Weltmann, K. D.; Wende, K.; Bogaerts, A.; Bekeschus, S. ROS from Physical Plasmas: Redox Chemistry for Biomedical Therapy. *Oxid. Med. Cell. Longevity* **2019**, *2019*, 1.

(16) Quiles, J. L.; Sánchez-González, C.; Vera-Ramírez, L.; Giampieri, F.; Navarro-Hortal, M. D.; Xiao, J.; Llopis, J.; Battino, M.; Varela-López, A. Reductive stress, bioactive compounds, redox-active metals and dormant tumor cell biology to develop redox-based tools for the treatment of cancer. *Antioxid. Redox Signaling* **2020**, *33*, 860.

(17) Barbosa, A. M.; Sarmento-Neto, J. F.; Menezes Filho, J. E. R.; Jesus, I. C. G.; Souza, D. S.; Vasconcelos, V. M. N.; Gomes, F. D. l.; Lara, A.; Araújo, J. S. S.; Mattos, S. S.; Vasconcelos, C. M. L.; Guatimosim, S.; Cruz, J. S.; Batinic-Haberle, I.; Araújo, D. A. M.; Rebouças, J. S.; Gomes, E. R. Redox-active drug, MnTE-2-PyP^{5+}, prevents and treats cardiac arrhythmias preserving heart contractile function. *Oxid. Med. Cell. Longevity* **2020**, *2020*, 1.

(18) Korge, P.; Calmettes, G.; Weiss, J. N. Increased reactive oxygen species production during reductive stress: The roles of mitochondrial glutathione and thioredoxin reductases. *Biochim. Biophys. Acta, Bioenerg.* **2015**, *1847*, 514−525.

(19) Zhang, P.; Sadler, P. J. Redox-Active Metal Complexes for Anticancer Therapy. *Eur. J. Inorg. Chem.* **2017**, *2017*, 1541−1548.

(20) Betanzos-Lara, S.; Habtemariam, A.; Sadler, P. J. Transfer Hydrogenation Reactions of Photoactivatable *N,N'*-Chelated Ruthenium(II) Arene Complexes. *J. Mex. Chem. Soc.* **2017**, *57*, 160−168.

(21) Liu, Z.; Romero-Canelón, I.; Qamar, B.; Hearn, J. M.; Habtemariam, A.; Barry, N. P. E.; Pizarro, A. M.; Clarkson, G. J.; Sadler, P. J. The Potent Oxidant Anticancer Activity of Organoiridium Catalysts. *Angew. Chem., Int. Ed.* **2014**, *53*, 3941−3946.

(22) Soldevila-Barreda, J. J.; Romero-Canelon, I.; Habtemariam, A.; Sadler, P. J. Transfer hydrogenation catalysis in cells as a new approach to anticancer drug design. *Nat. Commun.* **2015**, *6*, 6582−6590.

(23) Chen, F.; Soldevila-Barreda, J. J.; Romero-Canelón, I.; Coverdale, J. P. C.; Song, J. I.; Clarkson, G. J.; Kasparkova, J.; Habtemariam, A.; Brabec, V.; Wolny, J. A.; Schünemann, V.; Sadler, P. J. Effect of sulfonamidoethylenediamine substituents in Ru^{II} arene anticancer catalysts on transfer hydrogenation of coenzyme NAD^+ by formate. *Dalton Trans.* **2018**, *47*, 7178−7189.

(24) Chen, F.; Romero-Canelón, I.; Soldevila-Barreda, J. J.; Song, J. I.; Coverdale, J. P. C.; Clarkson, G. J.; Kasparkova, J.; Habtemariam, A.; Wills, M.; Brabec, V.; Sadler, P. J. Transfer Hydrogenation and Antiproliferative Activity of Tethered Half-Sandwich Organoruthenium Catalysts. *Organometallics* **2018**, *37*, 1555−1566.

(25) Kou, L.; Sun, R.; Xiao, S.; Zheng, Y.; Chen, Z.; Cai, A.; Zheng, H.; Yao, Q.; Ganapathy, V.; Chen, R. Ambidextrous approach to disrupt redox balance in tumor cells with increased ROS production and decreased GSH synthesis for cancer therapy. *ACS Appl. Mater. Interfaces* **2019**, *11*, 26722−26730.

(26) Ralph, S. J.; Nozuhur, S.; ALHulais, R. A.; Rodríguez-Enríquez, S.; Moreno-Sánchez, R. Repurposing drugs as pro-oxidant redox modifiers to eliminate cancer stem cells and improve the treatment of advanced stage cancers. *Med. Res. Rev.* **2019**, *39*, 2397−2426.

(27) Flórido, A.; Saraiva, N.; Cerqueira, S.; Almeida, N.; Parsons, M.; Batinic-Haberle, I.; Miranda, J. P.; Costa, J. G.; Carrara, G.; Castro, M.; Oliveira, N. G.; Fernandes, A. S. The manganese(III) porphyrin MnTnHex-2-PyP^{5+} modulates intracellular ROS and breast cancer cell

migration: Impact on doxorubicin-treated cells. *Redox Biol.* **2019**, *20*, 367−378.
(28) Batinic-Haberle, I.; Tome, M. E. Thiol regulation by Mn porphyrins, commonly known as SOD mimics. *Redox Biol.* **2019**, *25*, 101139.
(29) Krasnovskaya, O.; Naumov, A.; Guk, D.; Gorelkin, p.; Erofeev, A.; Beloglazkina, E.; Majouga, A. Copper coordination compounds as biologically active agents. *Int. J. Mol. Sci.* **2020**, *21*, 3965.
(30) Basu, U.; Roy, M.; Chakravarty, A. R. Recent advances in the chemistry of iron-based chemotherapeutic agents. *Coord. Chem. Rev.* **2020**, *417*, 213339.
(31) Rilak, A.; Bratsos, I.; Zangrando, E.; Kljun, J.; Turel, I.; Bugarčić, Ž. D.; Alessio, E. New Water-Soluble Ruthenium(II) Terpyridine Complexes for Anticancer Activity: Synthesis, Characterization, Activation Kinetics, and Interaction with Guanine Derivatives. *Inorg. Chem.* **2014**, *53*, 6113−6126.
(32) Huang, H.; Zhang, P.; Chen, Y.; Qiu, K.; Jin, C.; Ji, L.; Chao, H. Synthesis, characterization and biological evaluation of labile intercalative ruthenium(II) complexes for anticancer drug screening. *Dalton Trans.* **2016**, *45*, 13135−13145.
(33) Mijatović, A.; Šmit, B.; Rilak, A.; Petrović, B.; Čanović, D.; Bugarčić, Ž. D. NMR Kinetic Studies of the Interactions between $[Ru(terpy)(bipy)(H_2O)]^{2+}$ and some Sulfur-Donor Ligands. *Inorg. Chim. Acta* **2013**, *394*, 552−557.
(34) Mijatović, A. M.; Jelić, R. M.; Bogojeski, J.; Bugarčić, Ž. D.; Petrović, B. Kinetics, Mechanism, and Equilibrium Studies of the Reactions between a Ruthenium(II) Complex and some Nitrogen- and Sulfur-Donor Nucleophiles. *Monatsh. Chem.* **2013**, *144*, 1489−1498.
(35) Huang, H.; Zhang, P.; Chen, Y.; Ji, L.; Chao, H. Labile ruthenium(II) complexes with extended phenyl-substituted terpyridyl ligands: synthesis, aquation and anticancer evaluation. *Dalton Trans.* **2015**, *44*, 15602−15610.
(36) Notaro, A.; Gasser, G. Monomeric and dimeric coordinatively saturated and substitutionally inert Ru(II) polypyridyl complexes as anticancer drug candidates. *Chem. Soc. Rev.* **2017**, *46*, 7317−7337.
(37) Poynton, F. E.; Bright, S. A.; Blasco, S.; Williams, D. C.; Kelly, J. M.; Gunnlaugsson, T. The development of ruthenium(II) polypyridyl complexes and conjugates for in vitro cellular and in vivo applications. *Chem. Soc. Rev.* **2017**, *46*, 7706−7756.
(38) Chrzanowska, M.; Katafias, A.; Impert, O.; Kozakiewicz, A.; Surdykowski, A.; Brzozowska, A.; Franke, A.; Zahl, A.; Puchta, R.; van Eldik, R. Structure and reactivity of $[Ru^{II}(terpy)(N\text{^}N)Cl]Cl$ complexes: consequences for biological application. *Dalton Trans.* **2017**, *46*, 10264−10280.
(39) Kern, S.; van Eldik, R. Mechanistic insight from activation parameters for the reaction of a ruthenium hydride complex with CO_2 in conventional solvents and an ionic liquid. *Inorg. Chem.* **2012**, *51*, 7340−7345.
(40) Housecroft, C. E.; Sharpe, A. G. *Inorganic Chemistry*, 4th ed.; Pearson Education Ltd., 2012; p 188.
(41) Kieslich, G.; Sun, S.; Cheetham, A. K. Solid-state principles applied to organic−inorganic perovskites: new tricks for an old dog. *Chem. Sci.* **2014**, *5*, 4712−4715.
(42) Wang, W.-H.; Xu, S.; Manaka, Y.; Suna, Y.; Kambayashi, H.; Muckerman, J. T.; Fujita, E.; Himeda, Y. Formic acid dehydrogenation with bioinspired iridium complexes: A kinetic isotope effect study and mechanistic insight. *ChemSusChem* **2014**, *7*, 1976−983.
(43) Butt, H. J.; Kappl, M. *Surface and Interfacial Forces*, 2nd ed.; Wiley-VCH: Weinheim, Germany, 2018.

https://dx.doi.org/10.1021/acs.inorgchem.0c01613
Inorg. Chem. 2020, 59, 14944−14953